

# A State-of-the-Art Review on Direct Welding of Polymer to Metal for Structural Applications: Part 2 – Joint Design and Property Characterization

Direct welding of polymer to metal is not only possible; it also shows potential for applications in mass-production environments

BY A. S. KHAN, P. DONG, F. LIU, AND Y. ZHANG

## Abstract

Structural lightweighting through the effective use of multiple materials has received increasing attention for fulfilling today's demands for environmental sustainability in transportation systems. Direct dissimilar material joining methods (versus, e.g., traditional adhesive bonding or mechanical fastening) have become increasingly desirable since they offer process simplicity, production efficiency, and hermetic sealing, among others. In Part 1 of this two-part article, we provided a critical assessment of the state-of-the-art research and promising direct dissimilar material joining techniques reported over the last decades, with a particular emphasis on their potential for structural applications. As such, in Part 2, recent advances in advanced joint design and modeling methods for enabling optimum joint design for joint ability and joint performance are presented along with some detailed examples for demonstrating their potential impacts on industrial applications. Finally, recommendations on future research and development directions are outlined for supporting the industry's drive towards multi-material lightweighting.

## Keywords

- Dissimilar Materials Joining
- Polymer to Metal Direct Welding
- Welding
- Joint Property
- Chemical Bonding

## Introduction

As discussed in Part 1 of this two-part review article (Ref. 1), in addition to the need to ensure adequate chemical bonding at the polymer and metal interface as a result of direct joining methods, effective methodologies for extracting joint properties from simple lab specimen testing are also of critical importance for supporting computer-aided engineering (CAE) evaluation of multi-material structures for industrial applications.

Some of the direct polymer-to-metal joining methods that are discussed in Part 1 (Refs. 2–7) of this article have shown a great deal of potential for consideration in the manufacture of advanced lightweight structures. However, one additional major challenge remains: how to determine the mechanical properties of these joints in such a way that these properties can be used in the design and evaluation of actual structures. Most of the investigations have relied on simple lap shear (Fig. 1A) or coach peel (Fig. 1B) by performing either static tensile strength or fatigue tests. The resulting test data are typically presented in terms of nominal stress ( $F/A$ ) corresponding to load at failure, where  $A$  can be either defined as the loaded base plate cross-section area or the bonded area at the dissimilar material interface of a simple lab specimen, depending upon where the failure occurs in the test. As such, the test data cannot be directly adopted in a finite element (FE) model for structural design and optimization purposes. This is because, in actual structures, the load-carrying area  $A$  is typically ill-defined. To remove such limitations, the test data based on  $F/A$  obtained from simple lab specimens must be transformed into a joint-level property (e.g., tensile strength or fatigue strength). This would typically require rigorous mechanics-based modeling (e.g., through FE analysis). The major difficulty in performing FE analysis for welded joints is suppressing mesh-size-induced sensitivity when stresses are computed at sharp corner locations (see the red arrow lines in Fig. 1) where stress and strain possess singularity. This is illustrated in Fig. 2, in which two lap shear

<https://doi.org/10.29391/2024.103.013>

specimens were analyzed using commercial code ABAQUS (Ref. 8). The stresses at the sharp corner locations suffered severe mesh size sensitivity, just like in welded components as discussed in recent publications (Refs. 8–14). This issue must be resolved to reliably extract joint properties not only for evaluating dissimilar material joint design but also for optimizing structural performance in product development processes involving multi-materials.

## Joint Design and Joint Property Evaluation Methods

There have been two major developments in robust finite element methods for dealing with mesh-sensitivity problems caused by stress or strain singularity. One is referred to as the mesh-insensitive structural stress method (also known

as a traction structural stress method) for welded structures (Refs. 10, 11), and the other is the direct fracture mechanics approach (Ref. 8). For the latter, it would require a clearly defined crack size, which can be difficult to implement for structural design evaluations. Both methods are critically reviewed here, with a focus on their applications in determining critical joint design dimensions and their use in extracting joint properties for supporting engineering design.

## Mesh-Insensitive Traction Stress Method

There have been several publications over the last decade on the effectiveness of the mesh-insensitive traction stress method (Refs. 12–19) and its adoption in the ASME Boiler & Pressure Vessel international code (Ref. 20) for the design and evaluation of pressure vessel and piping components. The mechanical basis and computational procedures can be found in the references (Refs. 10, 13, 19) and will not be repeated here due to space limitations. In essence, the key reason behind the method’s mesh-insensitivity for computing stresses at sharp corner locations (see Figs. 1 and 2) is that nodal forces and moments from FE computation are used by imposing an equilibrium-equivalent argument if two-dimensional (2D) stress problems are considered or a work-equivalent argument in the form of a matrix equation if general 3D stress problems are considered. The effectiveness of a similar lap joint shown in Fig. 1A is summarized in Fig. 3. For the given loading conditions and the substrate thickness combination, the resulting normalized stress (i.e., stress concentration factor, SCF) by the remotely applied stress ( $F/A$ ) remains the same regardless of the relative element size ( $\Delta l/t$ ) used, as shown in Fig. 3C.

It should be noted that another advantage of the traction structural stress method is that the stress calculated

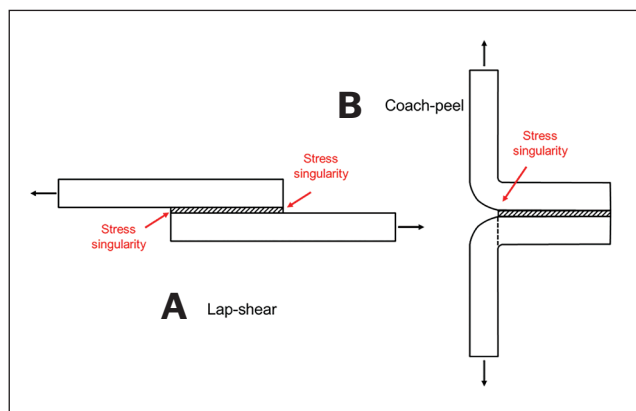


Fig. 1 – Existing testing schematics for dissimilar material joint property measurement (Ref. 8).

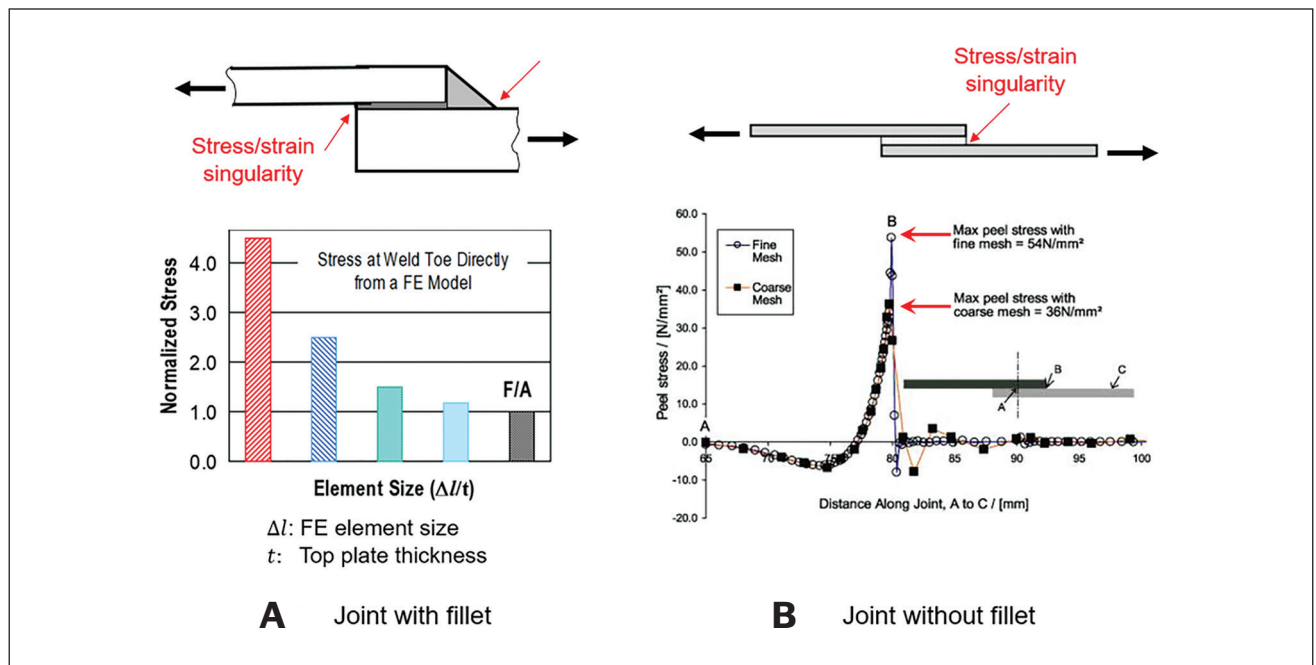


Fig. 2 – Effect of mesh size on joint strength evaluation due to inherent singularities.

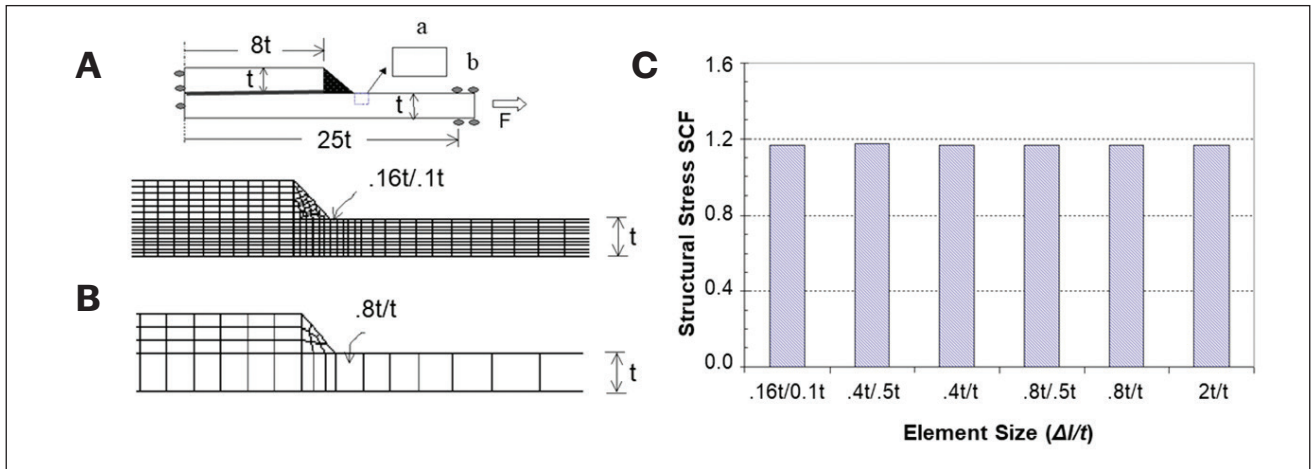


Fig. 3 – Traction-based mesh-insensitive structural stress and effect of mesh size on SCF (Refs. 9, 10).

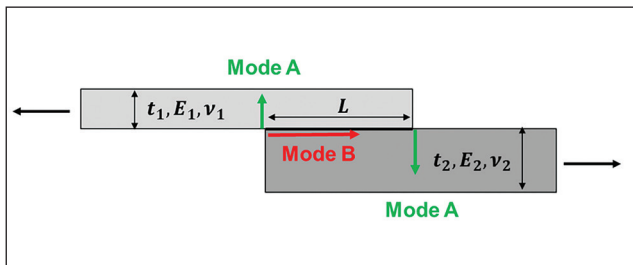


Fig. 4 – Failure modes in a typical bi-material joint.

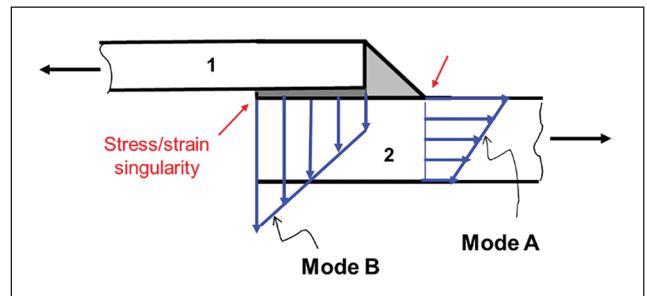


Fig. 5 – Illustration of traction stress definition controlling failure Mode A vs. B.

has a clear definition in terms of the failure mode (position and orientation) being considered. The traction structural stress results given in Fig. 3C correspond to failure initiated at the fillet corner (often referred to as toe) position into base plate thickness, referred to as failure Mode A. As explained in Fig. 4, the traction structural stress can be computed for Mode A, which has two possibilities, while Mode B represents interfacial failure (Refs. 8, 21, 22). Mode A is controlled by normal traction stress along its arrow line with respect to each of the substrate thicknesses. Mode B is controlled by the interfacial traction stress along the arrow line along the interface between Substrates 1 and 2, as further illustrated in Fig. 5. More detailed discussions on fillet welded components on how to treat Mode A versus Mode B failure mode can be found in Refs. 22–25.

## Joint Strength Property

For the dissimilar material joints, Liu et al. (Ref. 26) used the mesh-insensitive traction stress method discussed above to prove that PA66/AL 6061 joint shear strengths were essentially the same (up to about 5%) as welding speed varied from 1 m/min to 5 m/min (see Fig. 8B), even though the nominal shear strengths measured in F/A exhibited a significant variation up to 22% (see Fig. 8A). The joint cross-section profiles are shown in Fig. 6, corresponding to welding speeds 1 m/min, 3 m/min, and 5 m/min, respectively. Upon closer examination, the only difference among the three welding conditions given in Fig. 6 was the fillet size (see the arrow

lines). After the actual fillet sizes were considered in their finite element models, as shown in Fig. 7, the shear traction stresses computed corresponding to interfacial failure (i.e., Mode B, as described in Fig. 4) between PA66 and aluminum substrate were used for correlating the same test data given in Fig. 8A. This was done by multiplying the shear traction stress SCFs corresponding to the joint fillet profiles shown in Fig. 7 against their respective F/A values in Fig. 8A. The results are shown in Fig. 8B, which shows that all three welding conditions exhibited the same joint shear strengths within a scatter band of 5%. The shear strengths so calculated offer transferability, regardless of test specimen geometries and loading conditions, and, therefore, can be directly used in complex structural models for design and performance optimization purposes.

As another example of demonstrating the effectiveness of the mesh-insensitive traction stress method in interpreting joint strength test data, we considered the test specimens shown in Khan et al. (Ref. 6) for GFRP-PP to aluminum alloy 6061 joints, which resulted in Mode A failure along the PP base plate/material width (or BM failure). Although these specimens are of spot weld types, their Mode A failures along the PP base plate can be treated as 2D traction stress problems for illustration purposes here, so that simple closed-form analytical solutions can be readily obtained for gaining insights into how the mesh-insensitive traction method described above works.

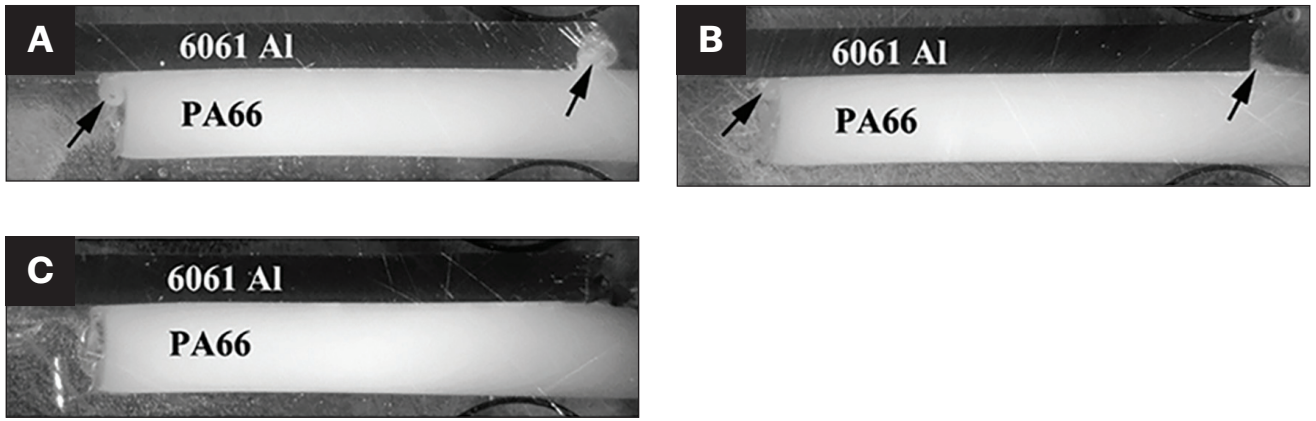


Fig. 6 – Fillet formation in PA66/AA6061 joint (Ref. 26).

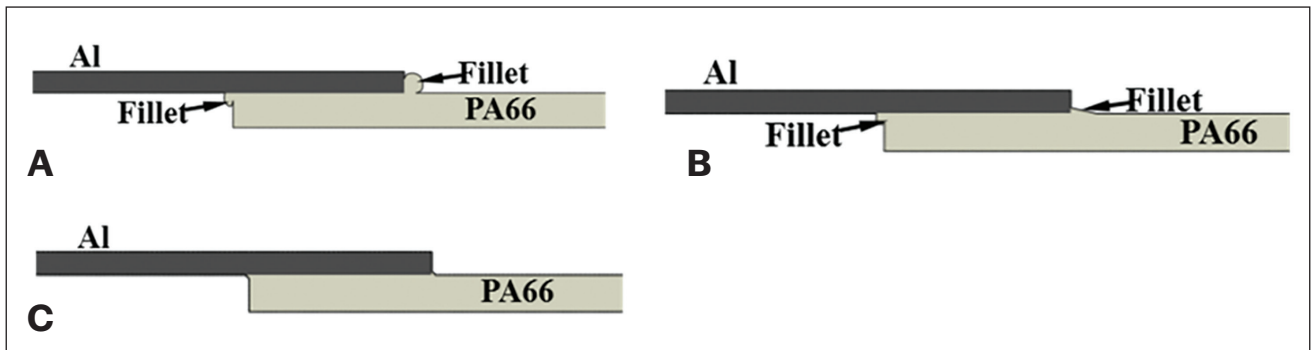


Fig. 7 – Fillet feature approximations for FE modeling using mesh-insensitive structural stress method (Ref. 26).

**Table 1 – Test data and corresponding membrane and total traction structural stress values**

Sample	$\sigma_m / S$	$(\sigma_m + \sigma_b) / S$
Sample-1	0.50	1.59
Sample-2	0.52	1.67
Sample-3	0.53	1.70

As shown in Fig. 9, the equilibrium condition with respect to moments leads to:

$$M_1 = P \times \left( \frac{t_1 + t_2}{2} - \frac{t_1}{2} \right) = \frac{P t_2}{2} \quad (1)$$

$$M_2 = P \times \left( \frac{t_1 + t_2}{2} - \frac{t_2}{2} \right) = \frac{P t_1}{2} \quad (2)$$

where  $P$  represents the applied line load (i.e., remote load divided by Substrate 2 width) at failure. Then, the traction

structural stress corresponding to a given failure mode is a linear combination of the membrane and bending stresses. For the cases shown in Fig. 9, the traction structural stress acting on the planes indicated by Line A-A with respect to substrate-1 (AA 6061) and Line B-B with respect to substrate-2 (PP) can be expressed for per unit specimen width (into the paper) as:

$$\sigma_{s1} = \sigma_{m1} + \sigma_{b1} = \frac{P}{t_1} + 6 \frac{M_1}{t_1^2} \quad (3)$$

and

$$\sigma_{s2} = \sigma_{m2} + \sigma_{b2} = \frac{P}{t_2} + 6 \frac{M_2}{t_2^2} \quad (4)$$

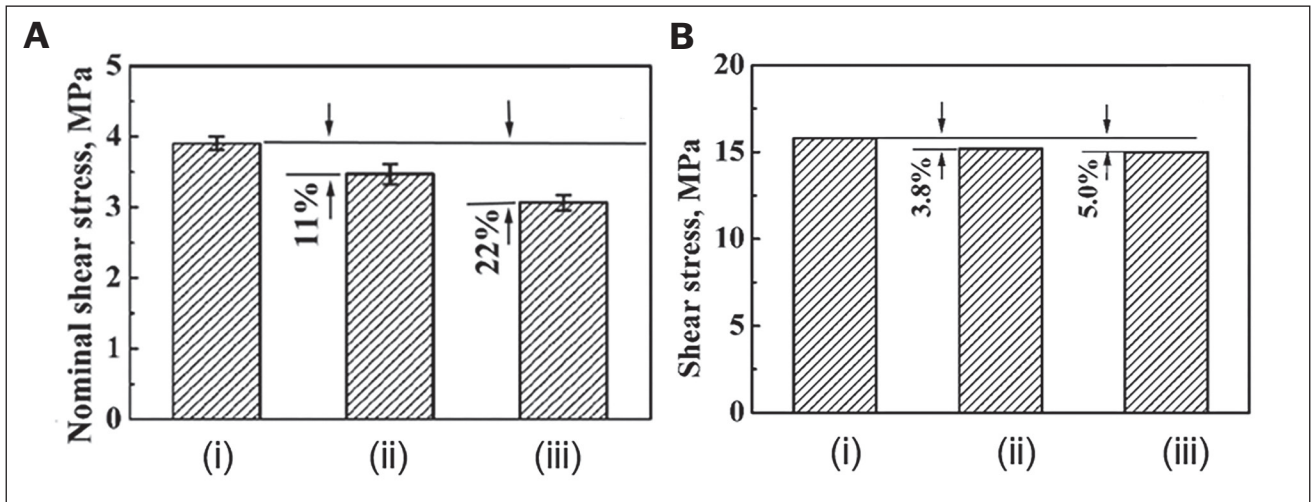


Fig. 8 – Traction stress-based joint shear strength results: A – Without considering the fillet features; B – after considering fillet features (Ref. 26).

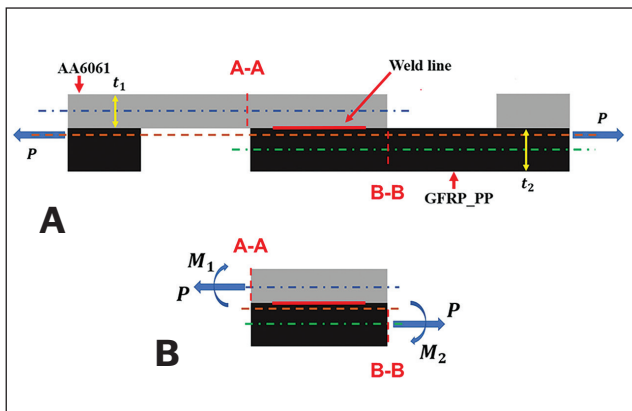


Fig. 9 – Analytical traction structural modeling of a lap shear joint specimen between AA 6061 and PP (GFRP).

respectively. Since  $t_1 = 2.00$  mm,  $t_2 = 2.70$  mm as given in Khan et al. (Ref. 6), the traction stress acting on the plane described by line B-B becomes  $\sigma_{s2} = 0.370P + 0.823P$ , which corresponds to the failure position observed in experiments.

To determine the static strength in terms of the membrane and bending parts of the traction stress given in Eq. 4, a well-established membrane and bending interaction diagram in terms of  $(\sigma_m + \sigma_b)/S$  versus  $\sigma_m/S$  (see ASME BPVC Section VIII Division 2) can be used here, as illustrated in Fig. 10, where  $S$  presents the tensile strength of PP from simple tensile strip tests. The curve and vertical straight line represent the theoretical static failure envelope. The AA 6061/PP joint test results from Khan et al (Ref. 6) expressed in terms of  $(\sigma_m + \sigma_b)/S$  versus  $\sigma_m/S$  are summarized in Table 1 below. These results are also plotted against the interaction diagram in Fig. 10, which shows that the failure envelope provides a reasonable estimation of the failure conditions observed from the test data, demonstrating the effectiveness of the mesh-insensitive traction stress in establishing test data transferability.

## Joint Fatigue Property

In addition to facilitating the extraction of joint static strength properties as discussed in the previous section, the traction structural stress method has been shown to be effective in the extraction of dissimilar material joint fatigue properties. One example along this line is the recent work by Zhang and Dong (Ref. 8) on modeling of adhesive-bonded test specimens in the form of lap shear (LS) and coach peel (CP) configurations, as shown in Fig. 11A. If the nominal stress ( $F/A$ ) range is used, the lap shear and coach peel test data follow their respective scatter band in the form of an S-N plot in a log-log scale (Fig. 11B). Once the traction structural stress method is used, the same test data points are collapsed into a single narrow band in Fig. 11C, indicating fatigue test data transferability. As a result, the single scatter band and its statistical values (e.g., mean  $-2\sigma$ ) can be used for structural fatigue evaluation of dissimilar material joints. Here,  $\sigma$  represents the standard deviation with respect to cycles to failure.

## Optimum Joint Design

In addition to joint property extraction, the optimum design of dissimilar material joints can be quantitatively determined using the new computational methods for structural applications. Both the computational fracture mechanics modeling and simplified analytical solutions recently developed by Zhang and Dong (Ref. 8) have shown that a threshold value exists about  $L/h \approx 2m$  beyond which fatigue driving force in terms of stress intensity factor ( $K_I$  corresponding to Mode-I, e.g., in coach peel tests, and  $K_{II}$  corresponding to Mode-II, e.g., in lap shear tests) remains constant, as shown in Fig. 12. This indicates that a further increasing in bond area size (e.g.,  $L$ ) no longer offers any additional fatigue capacity.

Indeed, the results shown in Fig. 11 have been confirmed by experimental test data ( $L/h \approx 3$ ), as shown in Fig. 13 for direct welding aluminum to steel by means of a new shear localization procedure described in Refs. 27–29.

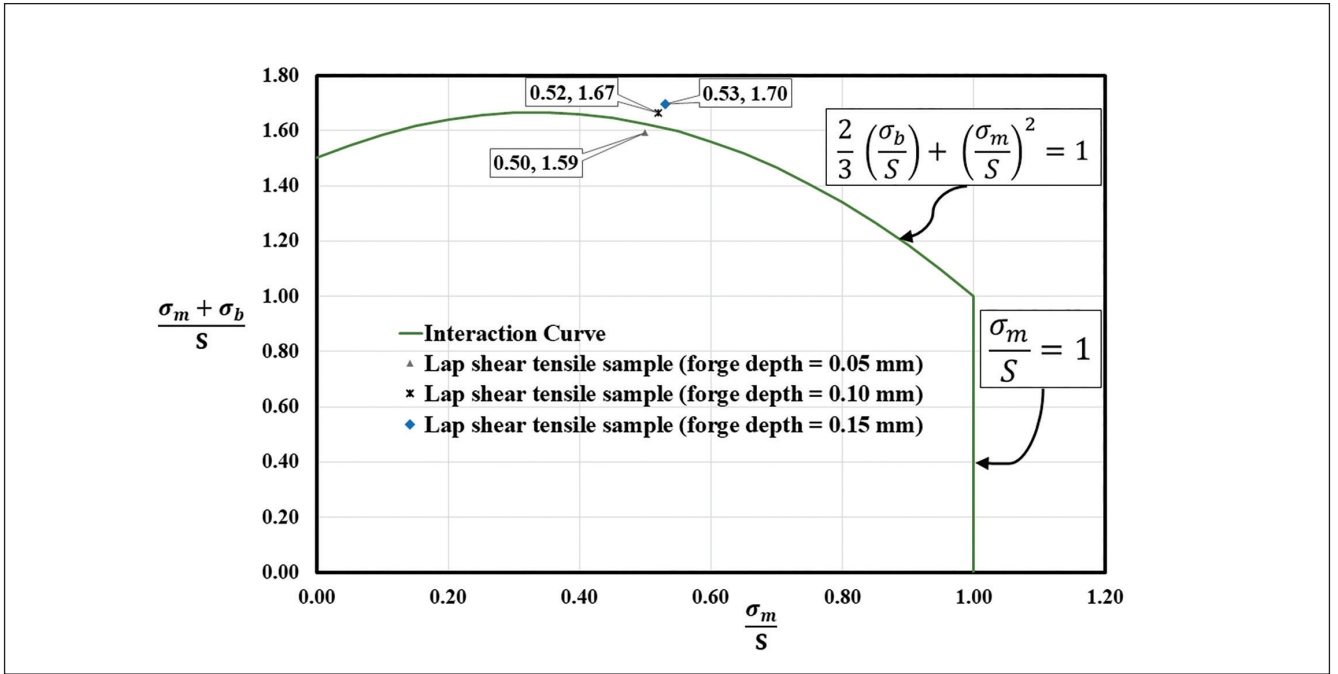


Fig. 10 – Membrane and bending interaction diagram for determining static strength and applications in interpreting AA 6061/PP (GFRP) joint test data.

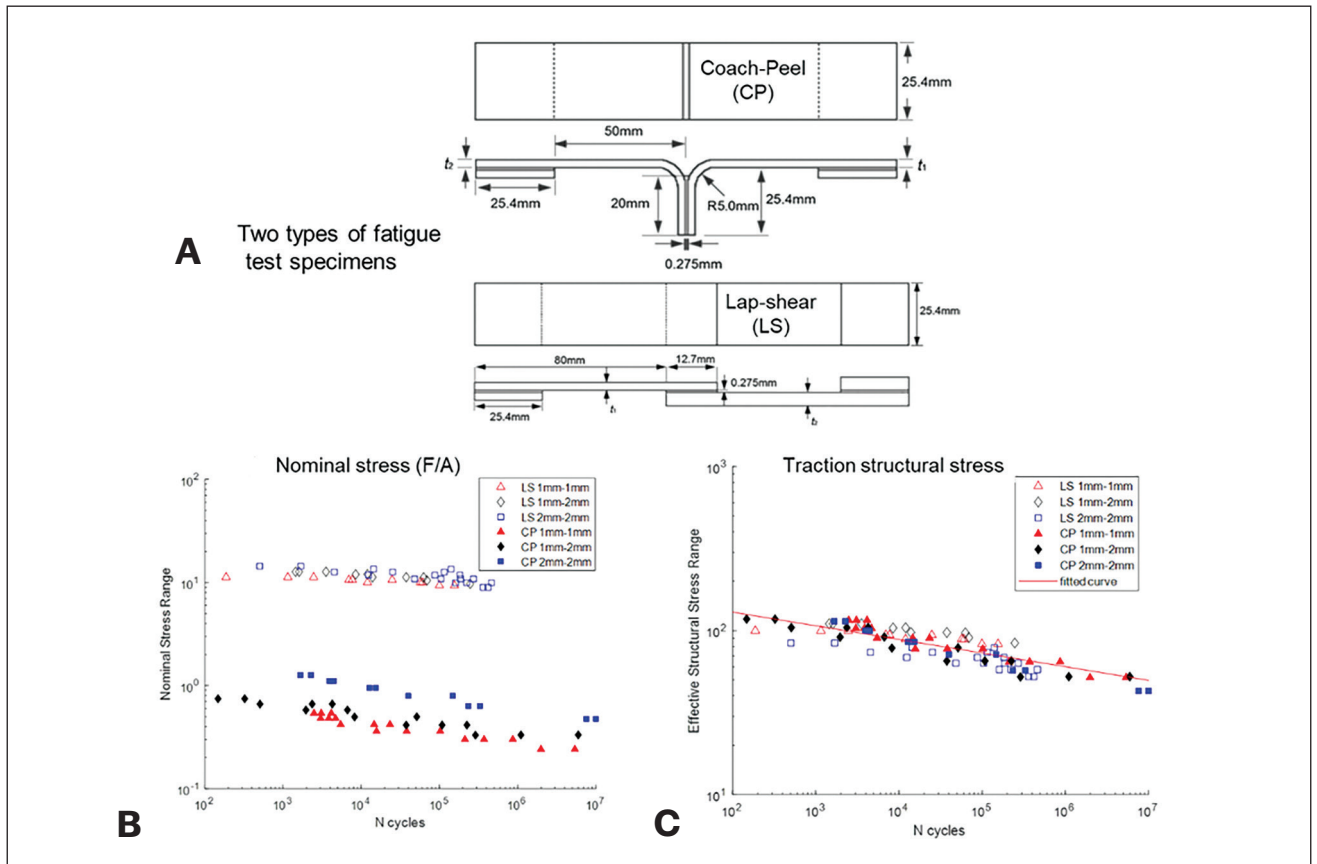


Fig. 11 – Traction structural stress modeling of fatigue in dissimilar material joints (Ref. 8).

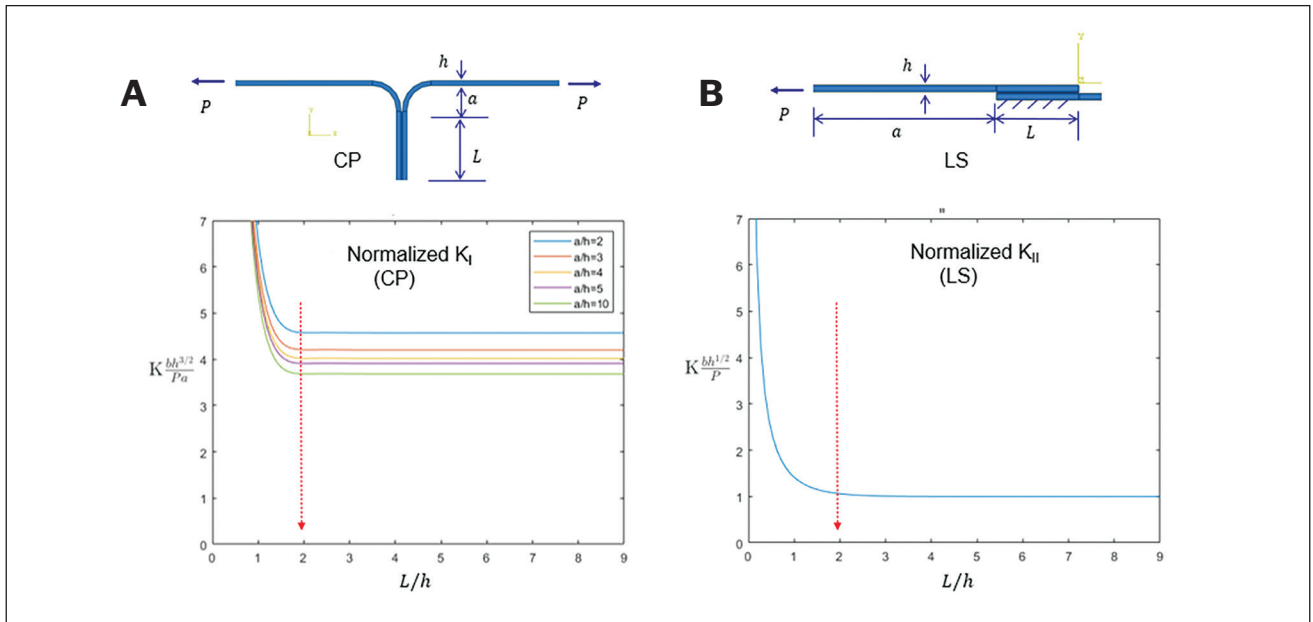


Fig. 12 – Effect of joining length on mode-I and mode-II stress intensity factor  $K$  (a fracture mechanics parameter).

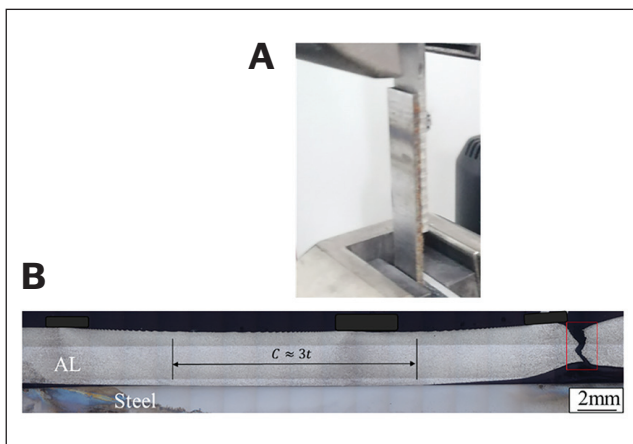


Fig. 13 – Validation of Mode A failure – aluminum to steel-welded lap shear tests.

Joint design rules can be simply stated as prevention of Mode B failure, if possible, regardless of static loading or fatigue loading. As such, Mode A failure provides the best load capacity under the given joint type and joint position, as illustrated in Fig. 14 covering both dissimilar and similar material joints. If the best load capacity is still not sufficient for a given structural application, alternative joint type and/or joint position needs to be considered, as discussed in Refs. 30 and 31.

## Unresolved Critical Issues for Industrial Applications

As discussed in Parts 1 and 2 of this article, although there have been numerous promising developments for achiev-

ing robust polymer-to-metal welding (e.g., either direct or through an intermediate carbonyl functional agent), industrial scale adoption of some of these dissimilar materials joining technologies is still in its infancy, particularly in a mass-production environment. To accelerate a broad adoption of these novel joining techniques for supporting the industry's drive toward multi-material lightweighting, three major hurdles need to be overcome. These are: (1) an improved understanding of C-O-M chemical bond development mechanisms and their controlling parameters; (2) effective procedures for extracting joint properties from simple lab test specimens for supporting computer-aided engineering of multi-material structures; (3) joint design guidelines for improved joint ability in process and joint performance in a structural context. These are further discussed below.

## Dominant Chemical Bond Formation Mechanism

The carbonyl functional group ( $C=O$ ) has been the most important chemical component for achieving the strong direct joining between the metals and the polymers (plastic). However, there are multiple theories on the bond formation mechanisms: Al-O-C type covalent bond formation between the aluminum and the polymer chain via carbonyl group, covalent bond formation between native aluminum oxide and the polymeric chain, and hydrogen bonding between the native aluminum oxide and the polymeric chain via hydrolysis of hydrocarbons in conjunction with the carbonyl group are among the top. The Van der Waals effect at the bonding interface is also considered a contributing factor. How to experimentally confirm one dominant bonding mechanism and to what extent over others under a given direct joining process condition remains challenging. The ability to do so is important for developing an optimized direct joining process

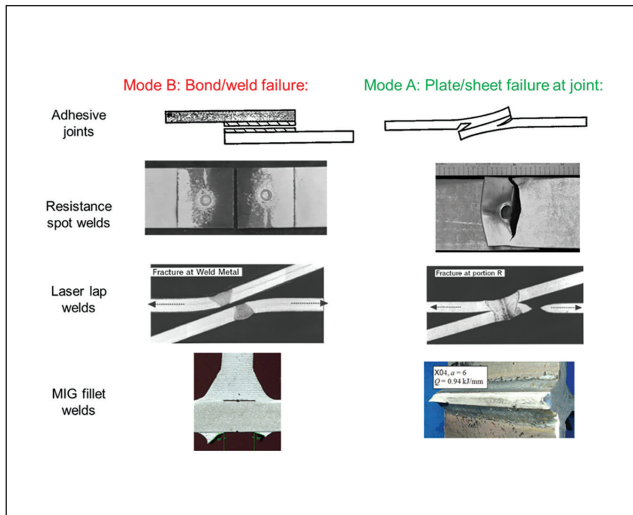


Fig. 14 – Failure Mode A vs. Mode B in various joint types in which Mode A offers the best static and fatigue load capacity and should be ensured through optimum joint sizing.

for promoting the uniformity and sufficient length scale of the resulting covalent chemical bond. In addition to capable measurement and characterization techniques, novel experimental approaches (e.g., the alumina/PA66 coating experiment by Liu et al. [Ref. 32]) to isolate and promote some of the bonding mechanisms can be effective for elucidating a favorable bond formation environment. Such insights played a key role in their subsequent process development (Refs. 6, 26).

## Joint Property Development

As discussed in Part 1, once a capable direct joining process has been established, it is important to establish a mechanics-based procedure for extracting mechanical properties from lab specimen test data for supporting CAE of multi-material structures. It should be emphasized here that any joint properties (e.g., joint tensile strengths and/or fatigue strengths [typically expressed in terms of S-N curve in stress life or E-N curve in strain life context]) must satisfy transferability requirements (i.e., properties that must exhibit invariance over specimen types; e.g., different thickness combinations of polymer and metal substrates) and loading mode (e.g., lap shear versus coach peel [see Fig. 11]). This aspect has not been adequately addressed. The recent developments in computational methods (e.g., the mesh-insensitive traction structural stress method) can be effective tools for extracting joint properties from simple lab specimen tests for use in CAE-based design optimization of complex structures. Once an effective joint property extraction procedure is in place, another benefit is that bond quality and its effect on a specific joint property parameter can be determined through either lap specimen testing or finite element modeling (see Figs. 10 and 11).

## Quantitative Joint Design Methods

The design of dissimilar material joints, particularly for direct joining methods (versus traditional mechanical fastening, as an example), is mostly done through empirical means today. As described in recent investigations (see Refs. 6, 8, 26), a proper joint design can significantly improve not only joint ability and cost in manufacturing but also joint performance in structures. Here, by joint design, we refer to three essential aspects: (1) joint location, (2) joint type (e.g., lap versus butt-seam); (3) joint detailing (bonding area size, end fillet (see Fig. 7), and nearby geometry (see Refs. 6, 8, 26). As demonstrated in Fig. 12, for a given dissimilar material combination, there exists an optimum interfacial bonding area or size, beyond which any benefit becomes rapidly diminished. As discussed earlier, advanced computational modeling methods are now available for quantitatively evaluating the three aspects above for structural applications. A longer-term objective should be the development of industry-wide joint design guidelines for typical dissimilar joint types and joining processes for mass-produced products for supporting a broader application of some of the advanced joining processes, which will facilitate confidence building, reduce development costs, and ensure product safety.

## Conclusion

A state-of-the-art assessment of polymer-to-metal direct joining research and promising techniques has been presented, with a particular emphasis on their applications for structural applications in the mass-produced marketplace. Direct welding of polymer to metal is not only possible but also shows the potential for applications in mass-production environments, in addition to its simplicity and excellent joint performance for some dissimilar material combinations. Coupled with some of the bond quality improvement techniques reviewed in this article, some mainstream structural applications are expected soon to achieve ever-increasingly structural lightweight goals by the transportation industry. Along this line, the research needs for supporting the technology transition were also highlighted, particularly around joint property development and effective methodologies for optimum joint design for joint ability and joint performance. Some of the recently developed computational methods were demonstrated through several detailed examples. Then, “using the right material at the right place” can become a reality for mass-produced products to meet today’s structural lightweighting needs.

## Acknowledgments

This work by Abdul Sayeed Khan, Pingsha Dong, and Yuning Zhang was partially supported by a National Science Foundation Grant (NSF CMMI 2126163) at the University of Michigan, Ann Arbor, Mich.

## References

1. Khan, A. S., Dong, P., Liu, F., and Zhang Y. 2024. A State-of-the-Art Review on Direct Welding of Polymer to Metal for Structural

Applications – Part I Promising Processes. *Welding Journal* 103(4): 117-s to 136-s. DOI: 10.29391/2024.103.011

2. Amancio-Filho, S. T., Bueno, C., dos Santos, J. F., Huber, N., and Hage, E. 2011. On the feasibility of friction spot joining in magnesium/fiber-reinforced polymer composite hybrid structures. *Materials Science and Engineering: A* 528: 3841–3848. DOI: 10.1016/j.msea.2011.01.085

3. Liu, F. C., Liao, J., and Nakata, K. 2014. Joining of metal to plastic using friction lap welding. *Materials & Design* 54: 236–244. DOI: 10.1016/j.matdes.2013.08.056

4. Kawahito, Y., Tange, A., Kubota, S., and Katayama, S. 2006. Development of direct laser joining for metal and plastic. *International Congress on Applications of Lasers & Electro-Optics* 25: 2604. DOI: 10.2351/1.5060840

5. Lambiase, F., Paoletti, A., Grossi, V., and Di Ilio, A. 2017. Friction assisted joining of aluminum and PVC sheets. *Journal of Manufacturing Processes* 29: 221–231. DOI: 10.1016/J.JMAPRO.2017.07.026

6. Khan, A. S., Liu, F., and Dong, P. 2023. Joining of metal and non-polar polypropylene composite through a simple functional group seeding layer. *Journal of Manufacturing Processes* 85: 90–100. DOI: 10.1016/J.JMAPRO.2022.11.022

7. Goushegir, S. M., dos Santos, J. F., and Amancio-Filho, S. T. 2014. Friction spot joining of aluminum AA2024/carbon-fiber reinforced poly(phenylene sulfide) composite single lap joints: Microstructure and mechanical performance. *Materials & Design* 54: 196–206. DOI: 10.1016/j.matdes.2013.08.034

8. Zhang, Y., Dong, P., and Pei, X. 2022. Fracture mechanics modeling of fatigue behaviors of adhesive-bonded aluminum alloy components. *Metals* 12(8): 1298. DOI: 10.3390/met12081298

9. Dong, P. 2001. A robust structural stress procedure for characterizing fatigue behavior of welded joints. *SAE International* 110: 89–100. DOI: 10.4271/2001-01-0086

10. Dong, P. 2001. A structural stress definition and numerical implementation for fatigue analysis of welded joints. *International Journal of Fatigue* 23: 865–876. DOI: 10.1016/S0142-1123(01)00055-X

11. Dong, P., & Hong, J. K. 2012. Fatigue of tubular joints: hot spot stress method revisited. *Journal of Offshore Mechanics and Arctic Engineering*. 134(3): 031602. DOI: 10.1115/1.4005188

12. Dong, P. 2003. A robust structural stress method for fatigue analysis of ship structures. *International Conference on Offshore Mechanics and Arctic Engineering*: 199–211. DOI: 10.1115/OMAEE2003-37313

13. Dong, P. 2005. A robust structural stress method for fatigue analysis of offshore/marine structures. *Journal of Offshore Mechanics and Arctic Engineering* 127: 68–74. DOI: 10.1115/1.1854698

14. Nie, C., and Dong, P. 2012. A traction stress based shear strength definition for fillet welds. *The Journal of Strain Analysis for Engineering Design* 47: 562–575. DOI: 10.1177/0309324712456646

15. Dong, P. 2001. A robust structural stress procedure for characterizing fatigue behavior of welded joints. *SAE International* 89–100. DOI: 10.4271/2001-01-0086

16. Wang, P., Pei, X., Dong, P., and Song, S. 2019. Traction structural stress analysis of fatigue behaviors of rib-to-deck joints in orthotropic bridge deck. *International Journal of Fatigue* 125: 11–22. DOI: 10.1016/j.ijfatigue.2019.03.038

17. Pei, X., Ravi, S. K., Dong, P., Li, X., & Zhou, X. 2022. A multi-axial vibration fatigue evaluation procedure for welded structures in frequency domain. *Mechanical Systems and Signal Processing* 167: 108516. DOI: 10.1016/j.ymsp.2021.108516

18. Kang, H. T., Dong, P., and Hong, J. K. 2007. Fatigue analysis of spot welds using a mesh-insensitive structural stress approach. *International Journal of Fatigue* 29: 1546–1553. DOI: 10.1016/j.ijfatigue.2006.10.025

19. Kyuba, H., and Dong, P. 2005. Equilibrium-equivalent structural stress approach to fatigue analysis of a rectangular hollow section joint. *International Journal of Fatigue* 27(1): 85–94. DOI: 10.1016/j.ijfatigue.2004.05.008

20. Dong, P., Hong, J. K., and De Jesus, A. M. P. 2006. Analysis of recent fatigue data using the structural stress procedure in ASME div 2 rewrite. *Journal of Pressure Vessel Technology* 129: 355–362. DOI: 10.1115/1.2748818

21. Zhang, L., Dong, P., Wang, Y., and Mei, J. 2022. A coarse-mesh hybrid structural stress method for fatigue evaluation of spot-welded structures. *International Journal of Fatigue* 164: 107109. DOI: 10.1016/j.ijfatigue.2022.107109

22. Xing, S., Dong, P., and Wang, P. 2017. A quantitative weld sizing criterion for fatigue design of load-carrying fillet-welded connections. *International Journal of Fatigue* 101: 448–458. DOI: 10.1016/j.ijfatigue.2017.01.003

23. Xing, S., Dong, P., and Threstha, A. 2016. Analysis of fatigue failure mode transition in load-carrying fillet-welded connections. *Marine Structures* 46: 102–126. DOI: 10.1016/j.marstruc.2016.01.001

24. Xing, S., Pei, X., Mei, J., Dong, P., Su, S., and Zhen, C. 2023. Weld toe versus root fatigue failure mode and governing parameters: A study of aluminum alloy load-carrying fillet joints. *Marine Structures* 88: 103344. DOI: 10.1016/j.marstruc.2022.103344

25. Wang, P., Pei, X., Dong, P., Yu, Y., and Li, X. 2020. Analysis of weld root fatigue cracking in load-carrying high-strength aluminum alloy cruciform joints. *International Journal of Fatigue* 139: 105735. DOI: 10.1016/j.ijfatigue.2020.105735

26. Liu, F. C., Dong, P., and Pei, X. 2020. A high-speed metal-to-polymer direct joining technique and underlying bonding mechanisms. *Journal of Materials Processing Technology* 280: 116610. DOI: 10.1016/j.jmatprotec.2020.116610

27. Liu, F. C., Dong, P., Zhang, J., Lu, W., Taub, A., and Sun, K. 2020. Alloy amorphization through nanoscale shear localization at Al-Fe interface. *Materials Today Physics* 15: 100252. DOI: 10.1016/j.mtphys.2020.100252

28. Liu, F. C., and Dong, P. 2021. From thick intermetallic to nanoscale amorphous phase at Al-Fe joint interface: roles of friction stir welding conditions. *Scripta Materialia* 191: 167–172. DOI: 10.1016/j.scriptamat.2020.09.031

29. Liu, F. C., Dong, P., Khan, A. S., Sun, K., Lu, W., Taub, A., et al. 2022. Amorphous interfacial microstructure and high bonding strength in Al-Fe bimetallic components enabled by a large-area solid-state additive manufacturing technique. *Journal of Materials Processing Technology* 308: 117721. DOI: 10.1016/j.jmatprotec.2022.117721

30. Dong, P. 2020. Quantitative weld quality acceptance criteria: an enabler for structural lightweighting and additive manufacturing. *Welding Journal* 99(2): 39–51. DOI: 10.29391/2020.99.004

31. Bingzhi, C., Zhengping, H., Dong, P., Song, S., and Wenzhong, Z. 2022. Quantitative fatigue evaluation of complex welded connections and application in a train traction motor frame component. *Proceedings of the Institution of Mechanical Engineers Part F Journal of Rail and Rapid Transit* 236: 1252–61. DOI: 10.1177/09544097221085329

32. Liu, F. C., Dong, P., Lu, W., and Sun, K. 2019. On formation of AIOC bonds at aluminum/polyamide joint interface. *Applied Surface Science* 466: 202–209. DOI: 10.1016/j.apsusc.2018.10.024

**ABDUL SAYEED KHAN, PINGSHA DONG** ([dongp@umich.edu](mailto:dongp@umich.edu)), **FENGCHAO LIU**, and **YUNING ZHANG** are with the Department of Naval Architecture and Marine Engineering, University of Michigan, Ann Arbor, Mich. **DONG** is also with the Department of Mechanical Engineering, University of Michigan, Ann Arbor, Mich.